# Binding mechanism of temporal soliton molecules

A. Hause, H. Hartwig, M. Böhm, and F. Mitschke*
*Universität Rostock, Institut für Physik, 18051 Rostock, Germany*
(Received 9 September 2008; published 10 December 2008)

Temporal optical soliton molecules were recently demonstrated; they potentially allow a further increase of data rates in optical telecommunication. We present a theoretical study aimed at an explanation of the mechanism responsible for the binding force. To this end we use a perturbation treatment in several variants. We find that the well-known soliton interaction as mediated by the optical Kerr effect, when suitably modified for chirped pulses, captures essential features like the existence of a stable equilibrium separation and small-scale oscillations around this point. Predictions of these models are compared to numerical simulations.

DOI: 10.1103/PhysRevA.78.063817 PACS number(s): 42.81.Dp, 42.65.Tg, 42.79.Sz

## I. INTRODUCTION

Today's telephone, telefax, and internet communication relies on the capability of optical fibers to transmit massive and ever-increasing amounts of information in the form of signaling light pulses. However, there is a fundamental limit to how much data a fiber can transmit per second. The limit is basically given by Shannon's channel capacity [1]

$$C = B \log_2(n),$$

where $B$ is the usable bandwidth and $n$ denotes the number of distinguishable values in each time slot. Taking into account the fiber's nonlinearity leads to some, but not to a major, correction to this result [2–4]. $B$ is set by the spectral range of the low-loss transmission of silica fiber and cannot be extended. Only the logarithmic factor describing the coding format allows some design freedom. In an analog format $n=1+S/N$, where $S$ is the signal power and $N$ the noise power. For binary digital systems, $n=2$—a trade of the capacity for robustness in the face of technical detriments.

The way for future commercial systems is paved by cutting-edge laboratory experiments which are always ahead in their data-carrying ability. The best experiments reported so far [5] are now within one order of magnitude of the Shannon limit for binary encoded data. In order to keep up with society's growing demand in the future, new concepts must be discussed and tested now.

Some recent experiments have successfully exploited coding schemes adopted from radio technology, such as quaternary phase shift keying and coherent detection, sometimes combined with polarization multiplexing [6,7]. However, in these concepts the fiber's inherent Kerr nonlinearity (absent in the transmission path of radio signals) is treated more as a nuisance. Arguably, an ultimately more elegant approach—which, however, is limited to a single bit per time slot as it stands now—embraces the fiber's nonlinearity to create solitons—i.e., light pulses which have the remarkable property that after perturbation they can readjust their shape. Solitons, or solitonlike pulses, can be transmitted even in dispersion-managed fiber [8]—i.e., fibers consisting of a periodic alternation of segments of fibers with opposite sign of the group velocity dispersion so that the resulting path-average dispersion is small. The suppression of four-wave mixing inherent in the dispersion management scheme minimizes neighboring-channel interference, and the natural robustness of solitons (their ability to self-heal after perturbations) makes this format particularly attractive. Indeed, a few commercial systems of this kind have been deployed recently.

A limitation of this technique is that neighboring solitons must not be located too close to each other to avoid the Kerr-mediated interaction [9,10]. Even though this effect is reduced in dispersion-managed fibers [11], it is still common practice to use soliton pulses several times narrower than the time slot because the interaction drops exponentially with increasing pulse separation. Like all other NRZ (no return to zero) schemes, this approach does not fully use the time axis, but rather reserves a sizable fraction of the time for safety distance; it also uses the spectral domain less than optimally because a pulse much shorter than the time slot will generate Fourier components at frequencies much higher than the clock rate, thereby enforcing a greater spectral distance to a neighboring channel. Therefore, this otherwise very robust and advantageous scheme will not be able to actually reach the Shannon limit.

We have recently demonstrated that compound states of solitons exist in dispersion-managed fiber. In [12] we showed that bound states involving two bright pulses exist: if two solitons are brought close to each other but with opposite phase, the attractive interaction turns repulsive at a particular separation which is of the same order as the pulse width, so that a stable equilibrium is created. Such double pulses were also found in numerical [13] and variational [14,15] computations. We showed by experiment and corresponding numerical simulation that these bound states survive in severely nonideal circumstances. Due to their ability to restitute their equilibrium separation after perturbation, we called these entities *soliton molecules*.

Soliton molecules might offer a solution to the overhead problem described above. Either one could use nonbinary coding within the time slot by picking symbols from the alphabet "no pulse," "single pulse," "double pulse." This scheme would unfold its full advantage if molecules of more than two pulses also existed. Both Ref. [13] and our own preliminary tests suggest that stable molecules of three bright pulses exist, but the stability of these and larger molecules

*fedor.mitschke@uni-rostock.de

 ©2008 The American Physical Society

needs to be established by a thorough investigation. Note that this concept would be very different from using intensity-modulated pulses which could have any desired amount of different intensities up to a limit set by the signal-to-noise ratio, but would suffer from all perturbations that plague analog systems. Soliton molecules, instead, inherit their self-healing property from fundamental solitons. Alternatively, and closer to current practice, one could exploit the existence of an equilibrium separation to pack conventional solitons much more closely than before—i.e., such that the time slot width coincides with the equilibrium separation. Interaction of the neighboring "bits" in the stream might then be virtually eliminated (but again, this needs to be thoroughly investigated and verified for all possible bit patterns).

Gabitov *et al.* [16] have presented a variational approach to find the shape of soliton molecules. Their results confirm the existence of an equilibrium separation, and even predict a secondary such equilibrium separation, which still awaits experimental confirmation. What has been missing so far from all discussions of soliton molecules was a comprehensible physical explanation for the mechanism providing the binding force.

We here present a perturbative treatment of the interaction of two solitons. For the record, Gordon formulated a linear perturbation treatment in close collaboration with Mollenauer in 2006 [17]. This approach indeed shows the existence of a stable equilibrium distance, and it does so in a very transparent way with intuitive appeal. Unfortunately, the position of the equilibrium point is not predicted with good quantitative precision.

In this paper we expand on the Gordon-Mollenauer approach in two ways: We extract information on the small-scale oscillations around this equilibrium, as they were observed before. More importantly, we extend the perturbation treatment beyond linear order, in order to determine whether higher-order terms give a noticeable contribution (they do) and whether an extended model can give better quantitative agreement (it cannot).

We will therefore show that quantitative agreement with numerical results remains less than perfect, whichever way the perturbation approach is pursued. The lack of quantitative agreement appears to be an inherent limitation of the perturbation approach. Nonetheless, it still has the undeniable advantage of conceptual clarity in showing the essential effects. This paper is organized as follows: In Sec. II the problem is stated, and since Gordon and Mollenauer did not publish their results, we begin by outlining their approach. Then, both the linear version and two variants of the perturbative approach are used to derive the interaction force, and hence the position of the stable equilibrium. In Sec. III we use the Gaussian pulse shape approximation to obtain specific values for the force. The resulting net effect is then obtained and compared to simulation results in Sec. IV. In Sec. V we turn to small-scale oscillations around that position and discuss the oscillation frequency.

## II. FORMULATING THE INTERACTION FORCES

It is clear enough that the phases of the optical fields are of central importance for the binding mechanism, yet ideas about how exactly the binding happens remained diffuse. A detailed analysis in [18] produced a full experimental characterization of both amplitude and phase structure of soliton molecules. The same publication also mentioned a very simple-minded concept of the interaction: Dispersion-managed solitons are well described by chirped Gaussian pulses [19–21]. A superposition of two such pulses at some temporal separation from each other can be constructed by adding the complex fields. Depending on chirp and separation, the resulting shape may exhibit extra structure in its power profile. The interaction force can be obtained as the net effect of all infinitesimal temporal slices across the resultant shape—i.e., an integral over the "local" force. Figure 1 demonstrates that this simple concept [shown in (b)] captures reality [as measured in (a)] amazingly well, which is encouragement to put this concept on a firm footing.

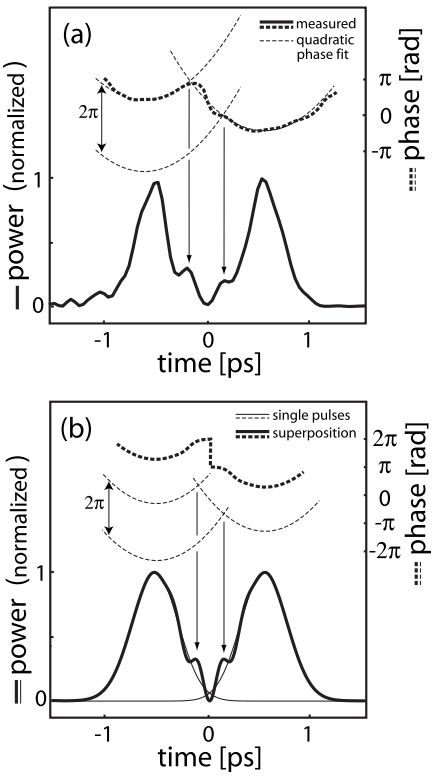


FIG. 1. (a) Reconstructed field of a double pulse, after [18]. The temporal pulse shape (solid line) and the temporal phase function (bold, dashed line) is shown. The fitted quadratic phase functions (thin, dashed line) for the single pulses show intersection points where constructive interference takes place and secondary peaks appear. (b) Superposition (bold, solid line) of two linearly cirped Gaussian pulses (thin, solid line). The intersection points of the single temporal phase functions denote the same positions of the secondary peaks.

In a lossless fiber, the propagation of an optical pulse is described by the nonlinear Schrödinger equation, here given in its normalized, dimensionless form

$$-iw_\zeta = \pm \frac{1}{2} w_{\tau\tau} + |w|^2 w, \tag{1}$$

where $w$ denotes the pulse envelope. Time $\tau$ is normalized to the $1/e$ half width of the launched pulse, $T_0$. $\zeta$ is the propa-

gation distance, scaled by the dispersion length $L_D=T_0^2/|\beta_2|$, where $\beta_2$ describes the dispersion.

Let $w=u+v$ be a superposition of two optical pulses. Inserting this into Eq. (1) and considering $v$ as a small perturbation of $u$ and vice versa, we obtain a symmetric pair of perturbed equations for the pulses $u$ and $v$:

$$-iu_\zeta = \pm\frac{1}{2}u_{\tau\tau} + |u|^2u + 2|u|^2v + u^2v^*, \tag{2}$$

$$-iv_\zeta = \pm\frac{1}{2}v_{\tau\tau} + |v|^2v + 2|v|^2u + v^2u^*. \tag{3}$$

We are seeking conditions under which the relative positions of the two pulses change. This can only happen through a change of the average soliton frequency $\langle\omega\rangle$: Due to dispersion, the frequency change translates into motion with respect to the frame of reference. The average frequency $\langle\omega\rangle$ can be expressed as [21,22]

$$\langle\omega\rangle = \frac{1}{W}\int_{-\infty}^{\infty}(-iu_\tau^*)u d\tau, \tag{4}$$

with the soliton energy $W=\int_{-\infty}^{\infty}u^*u\,d\tau$. The quantity relevant for our study is the acceleration which is proportional to $d\langle\omega\rangle/d\zeta$.

Using the fact that for an unperturbed soliton $\langle\omega\rangle=$const and $W=$const and truncating perturbation terms of higher than linear order one finds

$$\left.\frac{d}{d\zeta}\langle\omega\rangle\right|_{\text{lin pert}} = \frac{1}{W}\int_{-\infty}^{\infty}[u_\tau^*u(2u^*v+uv^*)]d\tau + \text{c.c.} \tag{5}$$

We will metaphorically refer to this as the "force," here written for linear perturbation on $u$. It is rearranged as

$$\left.\frac{d}{d\zeta}\langle\omega\rangle\right|_{\text{lin pert}} = \frac{1}{W}\int_{-\infty}^{\infty}[6\,\text{Re}(u_\tau^*u)\text{Re}(u^*v) - 2\,\text{Im}(u_\tau^*u)\text{Im}(u^*v)]d\tau. \tag{6}$$

In order to check whether higher-order corrections to this linear approach are negligible, we carry all higher-order perturbations of $v$ on $u$ and rewrite Eq. (2):

$$-iu_\zeta = \pm\frac{1}{2}u_{\tau\tau} + |u|^2u + 2|u|^2v + 2|v|^2u + u^2v^* + u^*v^2. \tag{7}$$

Then additional terms appear in Eq. (6):

$$\left.\frac{d}{d\zeta}\langle\omega\rangle\right|_{\text{full pert}} = \frac{1}{W}\int_{-\infty}^{\infty}[6\,\text{Re}(u_\tau^*u)\text{Re}(u^*v) - 2\,\text{Im}(u_\tau^*u)\text{Im}(u^*v) + 4\,\text{Re}(u_\tau^*u)|v|^2 + 2\,\text{Re}(u_\tau^*)\text{Re}(u^*v^2) - 2\,\text{Im}(u_\tau^*)\text{Im}(u^*v^2)]d\tau. \tag{8}$$

Both the linear and full perturbation treatments will be evaluated below, together with an alternative, in which one pulse moves in a modified potential, generated by the overlap of both pulses.

That variant is based on the following rationale: The soliton molecule has a symmetrical pulse shape, and one can consider each individual pulse in the pair as a replica of the other except for a time shift and a difference in phase (a possibly nonzero relative phase). Both modifications can be combined into some $a(\tau)$ so that the superposition of both pulses takes the form $w=u[1+a(\tau)]$. Now we get

$$-iu_\zeta = \pm\frac{1}{2}u_{\tau\tau} + |u|^2u + |u|^2u[2\,\text{Re}[a(\tau)] + |a(\tau)|^2], \tag{9}$$

and the force can then be expressed by

$$\left.\frac{d}{d\zeta}\langle\omega\rangle\right|_{\text{potential}} = \frac{2}{W}\int_{-\infty}^{\infty}\text{Re}(u_\tau^*u)|u|^2\{2\,\text{Re}[a(\tau)] + |a(\tau)|^2\}d\tau. \tag{10}$$

Still another route (which, however, leads to the same result; see below) would be to derive an equivalent force from the intensity envelope of the double pulse. Therefore we now use a generic ansatz for the optical pulse in the time domain: $u(\zeta,\tau)=|u(\zeta,\tau)|\exp\{i\phi(\zeta,\tau)\}$. The change of $\langle\omega\rangle$ is an effect of changing pulse shapes due to interference effects during propagation. This mixing of both pulses together with their nonlinear interaction is responsible for the change of the center frequency of a single pulse. Self-phase modulation (SPM) itself generates no change of the pulse envelope. The SPM-induced development of an arbitrary pulse in the temporal domain can be described by the evolution of the temporal phase function depending on the pulses intensity. In an approximation we now consider the case of a single perturbed pulse in a potential provided by the superposition of two pulses:

$$u(\zeta,\tau) = u(\zeta_0,\tau)e^{i|u+v|^2\zeta}. \tag{11}$$

From this point of view only the temporal phase function changes with $\zeta$. With $\partial|u|/\partial\zeta=0$, we have

$$\frac{d}{d\zeta}\left\{-i\left(\frac{\partial u^*}{\partial\tau}\right)u\right\} = -|u|^2\frac{\partial}{\partial\tau}\left(\frac{\partial\phi_{\text{nl}}}{\partial\zeta}\right). \tag{12}$$

With $\partial\phi_{\text{nl}}/\partial\zeta=|u+v|^2$ we obtain for the change of $\langle\omega\rangle$ the form

$$\left.\frac{d}{d\zeta}\langle\omega\rangle\right|_{\text{envelope}} = -\frac{1}{W}\int_{-\infty}^{\infty}|u|^2\frac{\partial}{\partial\tau}(|u+v|^2)d\tau, \tag{13}$$

basically the temporal derivative of the intensity shape of the superposition, weighted with the single-pulse intensity.

## III. EVALUATION AND COMPARISON

We have so far formulated the force in several approximations. Now we proceed to check for equilibrium positions in the soliton molecule. To this end we solve for the force-vs-separation behavior for all approximations and compare the results.

Specifically, we consider a superposition of two linear chirped Gaussian pulses $u$ and $v$ with temporal separation $T$,

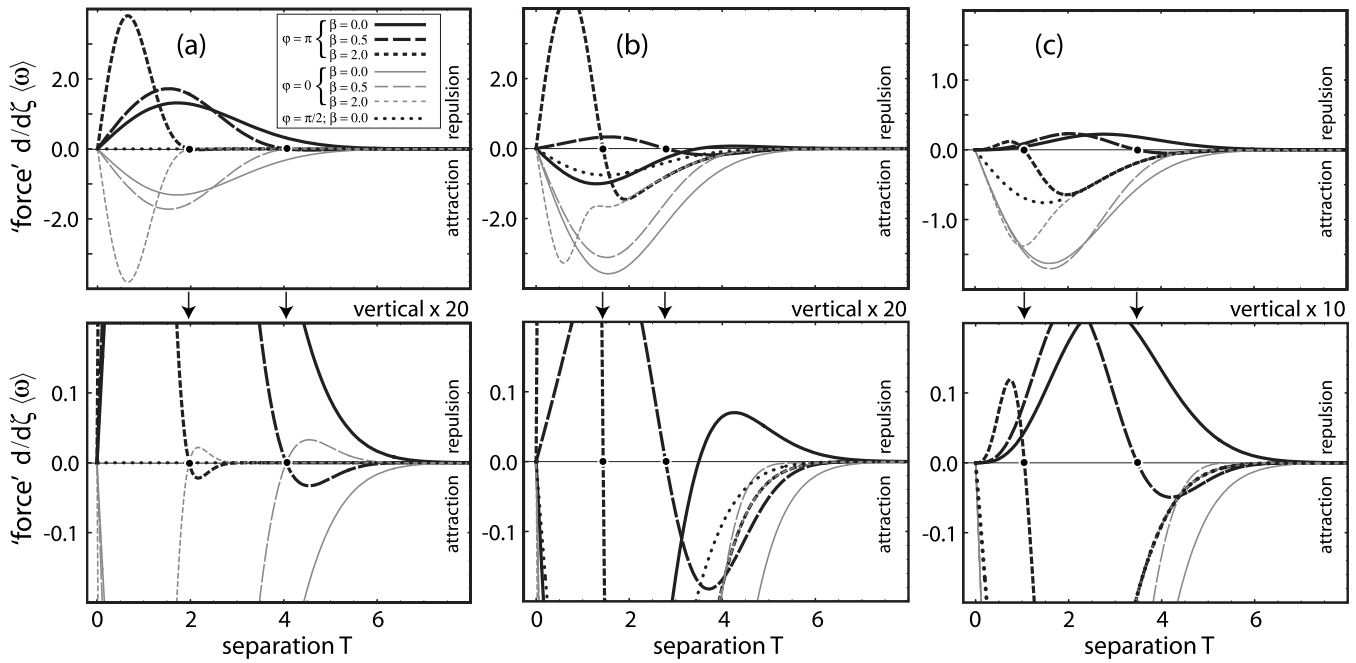


FIG. 2. Force acting on the single pulse $u$ according to (a) first-order perturbation theory, (b) higher-order perturbation theory, and (c) the modified potential model. Here the force $d/d\zeta\langle\omega\rangle$ is given in units of $W(\eta/\pi)$. The lower figures are on an expanded vertical scale to show more detail. Seven cases are shown: opposite phase ($\varphi=\pi$) for three chirp values, in phase for the same chirp values, and quadrature phase, unchirped. The pulse width parameter is $\eta=0.454$. Points on the horizontal axis, highlighted by arrows, mark stable equilibria. Positive (negative) values of the force imply repulsion (attraction) in the case of anomalous dispersion.

pulse width parameter $\eta$, linear temporal chirp parameter $\beta$, and relative phase $\varphi$. The center of $u$ is at $\tau=0$:

$$u = \sqrt{W}\left(\frac{\eta}{\pi}\right)^{1/4} \exp\left\{-\frac{(\eta+i\beta)}{2}\tau^2\right\},$$

$$v = \sqrt{W}\left(\frac{\eta}{\pi}\right)^{1/4} \exp\left\{-\frac{(\eta+i\beta)}{2}(\tau-T)^2+i\varphi\right\}. \quad (14)$$

The prefactor there is $\sqrt{W}(\eta/\pi)^{1/4}=N$; the soliton order $N$ is given in real-world units as $N^2=P_0T_0^2\gamma/|\beta_2|$.

With this we can find the force acting on $u$ at some particular position in the fiber; to obtain the net force for the soliton molecule, we will below integrate this local force over a whole dispersion period. Using the substitutions $A=-\eta(\tau^2-\tau T+\frac{1}{2}T^2)$ and $B=-\beta(-\tau T+\frac{1}{2}T^2)+\varphi$, we obtain for the linear perturbation treatment

$$\left.\frac{d}{d\zeta}\langle\omega\rangle\right|_{\text{lin pert}} = -W\left(\frac{\eta}{\pi}\right)\int_{-\infty}^{\infty}\{\tau\exp(A-\eta\tau^2) \times[6\eta\cos B+2\beta\sin B]\}d\tau. \quad (15)$$

If full perturbation terms are kept, this is described by

$$\left.\frac{d}{d\zeta}\langle\omega\rangle\right|_{\text{full pert}} = -W\left(\frac{\eta}{\pi}\right)\int_{-\infty}^{\infty}\{\tau\exp(A-\eta\tau^2) \times[6\eta\cos B+2\beta\sin B]+2\tau\exp(2A) \times\left[2\eta+\eta\cos\left(\tfrac{1}{2}\beta\tau^2+2B\right) +\beta\sin\left(\tfrac{1}{2}\beta\tau^2-2B\right)\right]\}d\tau. \quad (16)$$

In Fig. 2 we show a comparison of the linear and full perturbation treatments. In panel (a), Eq. (15) is plotted; in (b), Eq. (16). In either case, the initial separation of the two individual pulses is varied. For in-phase and opposite-phase situations, three different chirp values are shown. Also shown is the case of unchirped quadrature-phase pulses.

Not surprisingly, for large separations of the pulses ($T>6.5$ or so), there is no appreciable difference between the cases because the force vanishes anyway. However, in the more interesting case of the pulses approaching each other closely, the linear and full perturbative treatments show considerable differences. For linear perturbation [Fig. 2(a)] we distinguish the cases as follows.

*Opposite phase*. There is attraction which crosses over to repulsion as the separation is reduced; the zero-crossing point constitutes a stable equilibrium. For increasing chirp, this point moves inwards (towards smaller separation).

*In phase*. The figure is mirror symmetric to the opposite-phase case: Equilibria remain at the same positions, but stability is reversed.

*quadrature phase*. The force remains zero at all separations.

In contrast, for all-order perturbation [Fig. 2(b)], we find for the corresponding cases the following.

*Opposite phase*. While there are similarities, there is also an unstable equilibrium for the unchirped case.

*In phase*. Mirror symmetry is lost; now there is attraction everywhere.

*Quadrature phase*. There is attraction everywhere.

Quite generally it can be considered a test for the validity of linear perturbation when higher-order terms contribute

only negligibly. This is not the case here, and we have to accept that the perturbative treatment may remain quantitatively unprecise.

In view of this difficulty, we consider whether a modified perturbative approach might provide more accurate answers. We exploit the fact that in a lossless fiber, when only second-order dispersion and self-phase modulation are relevant effects, the soliton molecule is temporally fully symmetric. Therefore we now use a superposition of two linearly chirped Gaussian pulses $u$ and $u'$, similar to Eq. (14), but symmetrically displaced from the origin of the temporal frame of reference:

$$u = \sqrt{W}\left(\frac{\eta}{\pi}\right)^{1/4} \exp\left\{-\frac{(\eta+i\beta)}{2}\left(\tau+\frac{1}{2}T\right)^2 - i\frac{\varphi}{2}\right\}, \quad (17)$$

$$u' = \sqrt{W}\left(\frac{\eta}{\pi}\right)^{1/4} \exp\left\{-\frac{(\eta+i\beta)}{2}\left(\tau-\frac{1}{2}T\right)^2 + i\frac{\varphi}{2}\right\}. \quad (18)$$

Then, $u' = u\exp\{-(\eta+i\beta)\tau T + i\varphi\}$. Now we need to make some approximations concerning the pulse envelope. We consider the change of the power profile as slowly varying and therefore treat it as constant over short distances $\Delta\zeta$. Then we find the force as

$$\left.\frac{d}{d\zeta}\langle\omega\rangle\right|_{\text{potential}} = -W\left(\frac{\eta}{\pi}\right)\int_{-\infty}^{\infty} 2\exp\left\{-\eta\left(2\tau^2+\frac{1}{2}T^2\right)\right\} \times\left[\eta\left(\frac{1}{2}T-\tau\right)\right][2\exp(\eta\tau T) \times\cos(\varphi-\beta\tau T)+1]d\tau. \quad (19)$$

It can be shown that this result would also have been obtained if one had started with a modified and more symmetrical version of Eq. (7) as follows:

$$-iu_\xi = \pm\frac{1}{2}u_{\tau\tau} + |u|^2u + |v|^2u + (uv^* + u^*v)u. \quad (20)$$

Results from this approach are shown in Fig. 2(c). Again, at large separation nothing much happens. In the relevant regime we again distinguish the following cases.

*Opposite phase*. There are stable equilibrium points provided there is at least some chirp.

*In phase*. As before there is attraction everywhere.

*Quadrature phase*. As in full perturbation treatment, there is attraction everywhere.

While this is qualitatively similar to the cases treated above, there are differences in quantitative terms again.

To obtain the force from the intensity envelope, we use a superposition of two chirped Gaussian pulses $|u+v|^2$ and obtain after some straightforward calculation

$$|u+v|^2 = W\left(\frac{\eta}{\pi}\right)^{1/2}\left[\exp\left\{-\eta\left(\tau+\frac{1}{2}T\right)^2\right\} + \exp\left\{-\eta\left(\tau-\frac{1}{2}T\right)^2\right\} + 2\exp\left\{-\eta\left(\tau^2+\frac{1}{4}T^2\right)\right\}\cos(\beta\tau T-\varphi)\right]. \quad (21)$$

With the abbreviations $\tilde{A} = \eta\tau T$ and $\tilde{B} = \varphi - \beta\tau T$ and Eq. (13) we now get for the force

$$\left.\frac{d}{d\zeta}\langle\omega\rangle\right|_{\text{envelope}} = W\left(\frac{\eta}{\pi}\right)\int_{-\infty}^{\infty}\exp\left\{-2\eta\left(\tau^2+\frac{1}{4}T^2\right)\right\} \times[\eta(T-2\tau)(\exp(2\tilde{A})-1) - 2\exp\tilde{A}(2\eta\tau\cos\tilde{B}+\beta T\sin\tilde{B})]d\tau. \quad (22)$$

However, it turns out that this ansatz yields curves identical to those in Fig. 2(c). In other words, Eqs. (19) and (22) are equivalent. For unchirped pulses ($\beta=0$) the integrals of Eqs. (19) and (22) can be solved analytically and the force becomes

$$\left.\frac{d}{d\zeta}\langle\omega\rangle\right|_{\text{envelope}} = -W\left(\frac{\eta}{2\pi}\right)^{1/2}\eta T\left[\exp\left(-\frac{1}{2}T^2\eta\right) + \exp\left(-\frac{3}{8}T^2\eta\right)\cos\varphi\right]. \quad (23)$$

## IV. COMPARISON WITH NUMERICAL SIMULATIONS

We will now compare the predictions of the various versions of perturbation treatment with "real-world" numbers—i.e., the net effect of the force as found in numerical simulations. Comparison with experimental data is not meaningful for the following reason: It was shown in [12] that a full simulation including subtle effects like higher-order dispersion, splice loss, etc., comes remarkably close to the experimental values. Any theoretical model involves approximations, and in our treatment these extra complications are not considered. They can be turned off in numerics, but not in the experiment.

As a first step, we find the cumulative frequency shift $\Delta\langle\omega\rangle$ as the integral of the local "force" over one dispersion map period $\zeta_{\text{map}}$. In doing so it is essential to take into account the dynamic variation of the force as pulse durations, separations, peak powers, etc., evolve over the span of $\zeta_{\text{map}}$. In particular, the sign of the force will reverse where the sign of dispersion switches. The frequency change is accumulated as

$$\Delta\langle\omega\rangle = \int_{\zeta_{\text{map}}}\left.\frac{d\langle\omega\rangle}{d\zeta'}\right|_{\zeta'}d\zeta. \quad (24)$$

The net force, averaged over one dispersion map, is then given by $\Delta\langle\omega\rangle/\zeta_{\text{map}}$. By virtue of the fiber's dispersion, this

TABLE I. Parameters used for the simulation.

| | | |
|---|---|---|
| | $\tau_{\mathrm{FWHM}}=310$ fs | |
| | $E=65.55$ pJ | |
| | $P_0=198.73$ W | |
| $\beta_2^+=-26$ ps$^2$ km$^{-1}$ | | $\beta_2^-=62$ ps$^2$ km$^{-1}$ |
| $\gamma^+=0.902$ W$^{-1}$ km$^{-1}$ | | $\gamma^-=2.819$ W$^{-1}$ km$^{-1}$ |
| $L^+=4.97$ m | | $L^-=1.83$ m |
| | $\bar{\beta}_2=-2.3$ ps$^2$ km$^{-1}$ | |
| | $\bar{\gamma}=1.4$ W$^{-1}$ km$^{-1}$ | |
| | $S=3.77$ | |

frequency shift effects a positional shift which can be directly compared to numerical results.

For the numerical simulation we use a standard symmetrized split-step Fourier algorithm [23]. First, a single soliton was propagated to obtain the dynamic variation required for performing the integration in Eq. (24) (analytical expressions for this are not available). Parameter values were chosen to correspond to those in the first experiment [12] on soliton molecules. The dispersion values of the SSMF and IDF fibers (standard single-mode fiber and inverse dispersion fiber, respectively) are denoted by $\beta_2^{\pm}$; $\bar{\beta}_2$ is the path average value. $\gamma^{\pm}$ stand for the two nonlinearity parameters, $L^{\pm}$ for the lengths of the respective fiber segments. $L_{\mathrm{map}}=L^+ + L^-$ is the length of a dispersion map in correspondence to the dimensionless $\zeta_{\mathrm{map}}$ above, and $S$ is the map strength according to the definition

$$S = \frac{|\beta_2^+ - \bar{\beta}_2|L^+ + |\beta_2^- - \bar{\beta}_2|L^-}{\tau_{\mathrm{FWHM}}^2}. \tag{25}$$

Here we use the pulse's full temporal width at half maximum, $\tau_{\mathrm{FWHM}}=2\sqrt{\ln 2}T_0$, for Gaussian pulses. All parameter values are shown in Table I. The map strength used here corresponds to a case where the pulse shape of a dispersion-managed (DM) soliton is Gaussian to a very good approximation. We use real-world units from here on.

We start with a pulse shape which is close to the asymptotic shape. This can be obtained from propagation; the method of Nijhof *et al.* [24] speeds up convergence considerably. Then we perform a simulation of propagation over a single map period $L_{\mathrm{map}}$. In order to obtain $P_0(z)$ and $T_0(z)$ from the propagation data, we fit Gaussians to the actual shape. From a polynomial fit to the phase we also obtain the linear chirp parameter $\beta$ (the quadratic chirp parameter is also obtained, but used only for consistency checks). Figure 3 shows the evolution of $\beta(z)$ and $T_0(z)$ over $L_{\mathrm{map}}$. Strong breathing of the pulse shape and perfect recurrence after one dispersion map are plainly visible.

We have now obtained detailed information about the evolution of a single pulse and can proceed to constructing a pulse pair of two identical pulses, placed at a mutual separation $\sigma$ (the real world unit version of $T$ above). As the pair propagates, we can obtain the effective force for each position $z$ (see below). This force will set the two pulses into opposite relative motion. One should realize, however, that

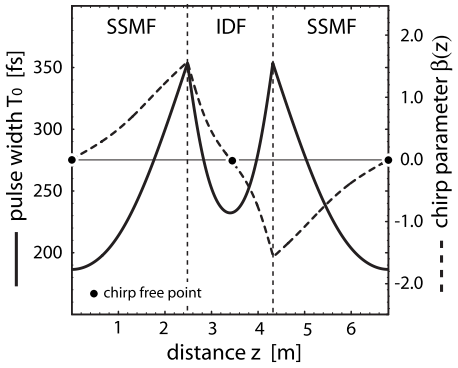


FIG. 3. Pulse width $T_0$ during propagation (solid line) and linear chirp parameter $\beta(z)$ (dashed line) as a function of distance $z$ over one period of the dispersion map. The dashed vertical lines mark the joints between fiber segments. The chirp-free points in the middle of each fiber segment are indicated by points. SSMF: standard single-mode fiber. IDF: inverse dispersion fiber.

(due to the frequency change involved) the relative phase remains constant in this motion. It turns out that the positional change is small and can be neglected (see below).

Let us mention three subtle technical points about the propagation simulation of the pulse pair: In the presence of the dynamical evolution of pulse width and chirp, we obtain a periodic change of the total energy of the pulse pair by construction. To correct for this artifact, the total energy (which is, of course, preserved) is normalized to the initial value at all positions $z$. This yields a corrected peak power $P'(z)$, which is used for the calculation of the force. Since the pulse width varies during propagation, the definition of the dispersion length $L_{\mathrm{D}}=T_0^2/|\beta_2|$ requires a remark. Group velocity dispersion is an entirely linear process and as such cannot produce spectral changes: it will affect only the temporal pulse shape. Therefore it is reasonable to refer $L_{\mathrm{D}}$ to some characteristic width, to render it a constant. A good choice is the width at the chirp-free point (see Fig. 3) where the pulses are unchirped and a single pulse would be Fourier limited. Thus we specify $L_{\mathrm{D}}$ using the value of $T_0$ at the chirp-free point in the respective fiber segment. In contrast, we treat the nonlinear length $L_{\mathrm{NL}}=1/(\gamma P')=1/[\gamma P'(z)]$ as a function of $z$.

We calculate the force for every distance $z$ by converting Eq. (22) to its equivalent in real-world units:

$$\left.\frac{d\langle\omega\rangle}{dz}\right|_{\mathrm{envelope}} = -\gamma P' \exp\left(-\frac{\sigma^2}{2T_0^2}\right) \times\left[\frac{\sigma}{\sqrt{2}T_0^2} - \frac{2}{\sqrt{\pi}T_0^3}\int_{-\infty}^{\infty}\Theta(t)dt\right], \tag{26}$$

where $\Theta(t)$ is an abbreviation for

$$\Theta(t) = \exp\left(-\frac{2t^2+t\sigma}{T_0^2}\right)[2t\cos\alpha + \beta\sigma\sin\alpha]; \tag{27}$$

$\alpha$ expresses the linear chirp-induced field oscillations of adjacent Gaussian pulses due to interference effects, and is given by

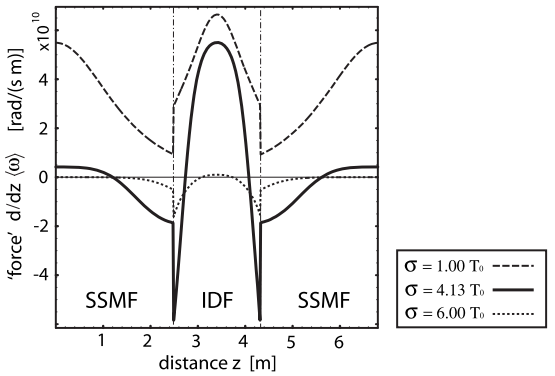


FIG. 4. Evolution of $d\langle\omega\rangle/dz$ in a single dispersion period. The behavior of double pulses with an initial separation of $\sigma=T_{0,z=0}$ (dashed), $\sigma=4.13T_{0,z=0}$ (solid line) und $\sigma=6T_{0,z=0}$ (dotted line) is shown.

$$\alpha = \frac{\beta\sigma}{T_0^2}t - \varphi. \tag{28}$$

The frequency shift of Eq. (26) defines the force at any position in the fiber. Its variation with $z$ is shown in Fig. 4 for three different separations. If the separation is quite large (dotted curve), the pulses have minimal overlap and an appreciable interaction occurs only near the splice points where the pulse width is maximum. If, on the other hand, the pulses are very close (dashed curve), the leading pulse is blueshifted and thus advanced everywhere (anomalous path average dispersion), whereas by symmetry the trailing pulse is retarded. As a net effect, there is repulsion.

To find the net force we consider the net frequency shift $\Delta\langle\omega\rangle$ during propagation over $L_{\text{map}}$. Here we need to integrate the local effect over the distance. This integration, of course, is done numerically. In between the cases just discussed there is a situation in which the net force vanishes (solid line). This defines the soliton molecule's equilibrium separation; for the parameters used here, we locate it at

$$\sigma_{\text{eq}} \approx 4.13T_{0,z=0}. \tag{29}$$

Above we have neglected the positional change of the pulses. This can now find its justification: A second integration of the force over distance yields the temporal shift which comes out as a few femtoseconds, when the separation is several picoseconds. This $10^{-3}$ change can indeed be neglected.

Let us quantitatively compare predictions from the three versions of the perturbation treatment. In Fig. 5 the net force of antiphase DM solitons is plotted as a function of initial separation. In all three cases, a stable equilibrium is predicted, but at slightly different positions at $3.31T_0(\approx 615$ fs), $4.13T_0(\approx 770$ fs), and $4.68T_0(\approx 870$ fs). This needs to be compared to the experimental and numerical result of 440 fs, which translates here to $2.37T_0$. We have to note that perturbation treatment in all variants overestimates the equilibrium position.

A peculiarity of the full perturbation treatment is the prediction of an unstable equilibrium point at somewhat smaller separation; there is no experimental evidence to the existence

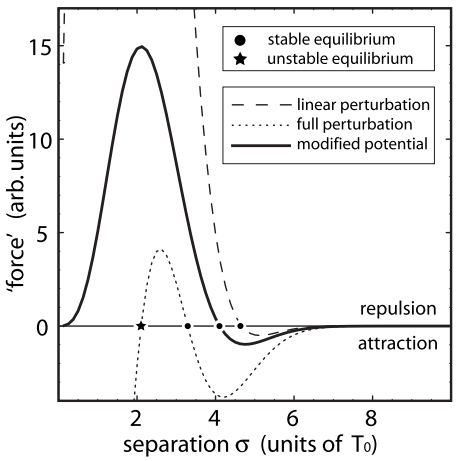


FIG. 5. Overview of the "forces" as obtained from the three models (linear perturbation, full perturbation, modified potential). The extended perturbation model shows an additional attraction of opposite phase DM solitons at very close separations. There is also an unstable equilibrium separation.

of such a point. The linear perturbation treatment has a different peculiarity: It alone predicts that forces always reverse sign when the relative phase is inverted, while both other approaches predict the existence of a regime where there is attraction for any value of the relative phase. With a full numerical simulation shown in Fig. 6 we demonstrate that such a situation does in fact exist. The figure compares the power profiles before (solid line) and after (dashed line) propagation through a long fiber (50 map periods) for in-phase, quadrature, and opposite-phase pulse pairs. One can clearly see that the pulses move toward each other in all cases. We verified that the same conclusion is found when one allows the net force found above for one map period to modify the initial values of $\sigma$ and $\langle\omega\rangle$ for the next period and so on.

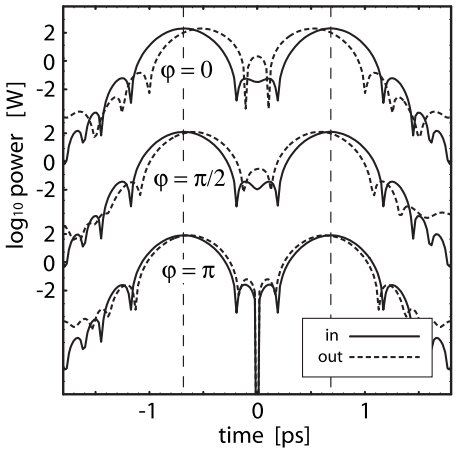


FIG. 6. Attraction of two DM solitons in dependence of their relative phase. The temporal profile is shown on a logarithmic power scale. A superposition of two solitons with parameters according to Table I was propagated over 50 dispersion periods. Soliton pairs have the strongest attraction when they are in phase and the weakest when they have opposite phase.

## V. OSCILLATIONS NEAR THE EQUILIBRIUM

Numerical simulations show that soliton molecules, when perturbed away from their equilibrium separation, oscillate around that point. From the treatment of the forces given above, we can now also find the restoring force near the equilibrium point and, hence, the oscillation period.

The net force $\Delta\langle\omega\rangle/L_{\mathrm{map}}$ describes the net frequency change per distance in $(\mathrm{rad\ s^{-1}})/\mathrm{m}$. Then,

$$\frac{\Delta\langle\omega\rangle}{L_{\mathrm{map}}}\bar{\beta}_2 = \frac{d^2}{dz^2}t_0, \tag{30}$$

where the temporal center of a single pulse is elongated from its equilibrium position by $t_0=(\sigma-\sigma_{\mathrm{eq}})/2$. For small excursions from equilibrium we may treat the molecule as a harmonic oscillator:

$$\frac{d^2}{dz^2}(\sigma-\sigma_{\mathrm{eq}}) + \Omega^2(\sigma-\sigma_{\mathrm{eq}}) = 0, \tag{31}$$

where $\Omega$ represents the frequency of the spatial oscillation around equilibrium. The spatial period in meters is then $2\pi/\Omega$. Note that $\Omega^2$ is equal to twice the slope of the curves in Fig. 5 at equilibrium because by virtue of symmetry both pulses contribute equally. Using Eq. (26) to calculate the "acceleration" of $u$ near the equilibrium distance with the parameters given above, we find an spatial oscillation period of $z_{\mathrm{osc}}\approx 286.6$ m corresponding to $z_{\mathrm{osc}}\approx 42.1L_{\mathrm{map}}$. Numerical simulations yield $z_{\mathrm{osc}}\approx 10L_{\mathrm{map}}$ dispersion periods. Of course, given the quantitative inaccuracies noted above, quantitative precision was not to be expected.

## VI. CONCLUSIONS

As noted above, we here used pulse shapes obtained with the help of the method of Nijhof *et al.* [24]. As an alternative, we already mentioned the method of Gabitov *et al.* [16], which is based on the Gabitov-Turitsyn-model of DM solitons [25]. Its basic idea is to average the evolution of the spectral phase function over an entire dispersion map. The spectrum is treated as slowly varying, which is justified if $L_{\mathrm{NL}}\gg L_{\mathrm{map}}$. The method aims at finding all sets of DM fibers for which the same stable solution of soliton molecules exists. It involves a reduction of all parameters to a single quantity called $\bar{d}_0$. An iterative procedure yields stable solutions for $\bar{d}_0$ from which the parameters of both the fiber line and the pulse shape fulfilling this solution can be calculated. This method is potentially very powerful, yet numerically demanding.

In our case the fiber parameters are already known so that the method of Gabitov *et al.* provided no advantage. Moreover, here $L_{\mathrm{NL}}\approx L_{\mathrm{map}}$ so that a condition of validity for the method of Gabitov *et al.* is violated. Therefore we did not use that method. Let us emphasize again that our interest was not to find the exact pulse shape: our intention was to understand the mechanism behind the binding force. The perturbation treatment is indeed successful in bringing it out in great clarity.

In summary we have investigated the adjacent soliton interaction in dispersion-managed fiber lines to identify the essential effects responsible for the binding mechanism of soliton molecules. We chose a perturbation approach because it has the advantage of being physically intuitive.

Linear perturbation turns out not to be fully satisfactory; therefore, we employ two refined versions thereof. The general behavior is captured very well by all versions, but the quantitative agreement with direct numerical simulations remains less than perfect.

The basic binding mechanism of soliton molecules emerges as follows: As is well established, pulses overlapping in constructive interference produce an enhanced power which, by way of the optical Kerr effect, causes an attraction. Similarly, destructive interference leads to repulsion. Here we deal with chirped pulses in a DM fiber. All pulse characteristics, including width and chirp, are oscillating, and the phase varies across the pulse. In the resulting oscillating interference condition different time slots within the pulses may have constructive; others, destructive interference. What counts is the resulting net effect for the interaction force. The perturbation treatment corroborates that there is indeed a stable equilibrium at a particular value of the pulse's mutual separation.

## ACKNOWLEDGMENTS

We are indebted to James P. Gordon and Linn F. Mollenauer who made their unpublished work available to us. We built on that, and we enjoyed fruitful discussions with them. This work was supported in the framework of DIP 6.6 (Deutsch-Israelische Projektpartnerschaft).

[1] C. E. Shannon, Bell Syst. Tech. J. **27**, 379 (1948); **27**, 623 (1948).
[2] P. P. Mitra and J. B. Stark, Nature (London) **411**, 1027 (2001).
[3] K.-P. Ho and J. M. Kahn, Channel capacity of WDM systems using constant-intensity modulation formats, in *Proceedings of the Optical Fiber Communications Conference*, edited by A. Sawchuk (Optical Society of America, OSA Trends in Optics and Photonics, 2002) Vol. 30, paper ThGG85.
[4] J. Tang, J. Lightwave Technol. **24**, 2070 (2006).
[5] A. H. Gnauck, G. Charlet, P. Tran, P. Winzer, C. Doerr, J. Centanni, E. Burrows, T. Kawanishi, T. Sakamoto, and K. Higuma, J. Lightwave Technol. **26**, 79 (2008).
[6] J. M. Kahn and K.-P. Ho, IEEE J. Quantum Electron. **10**, 259 (2004).
[7] P. J. Winzer and R. J. Essiambre, in *Optical Fiber Telecommunications V*, edited by I. P. Kaminow, T. Li, and A. E. Willner (Academic Press, San Diago, 2008).
[8] J. H. B. Nijhof, N. J. Doran, W. Forysiak, and F. M. Knox, Electron. Lett. **33**, 1726 (1997).
[9] J. P. Gordon, Opt. Lett. **8**, 596 (1983).

[10] F. M. Mitschke and L. F. Mollenauer, Opt. Lett. **12**, 355 (1987).
[11] P. V. Mamyshev and N. A. Mamysheva, Opt. Lett. **24**, 1454 (1999).
[12] M. Stratmann, T. Pagel, and F. Mitschke, Phys. Rev. Lett. **95**, 143902 (2005).
[13] A. Maruta, T. Inoue, Y. Nonaka, and Y. Yoshika, IEEE J. Sel. Top. Quantum Electron. **8**, 640 (2002).
[14] C. Paré and P.-A. Bélanger, Opt. Commun. **168**, 103 (1999).
[15] B.-F. Feng and B.-A. Malomed, Opt. Commun. **229**, 173 (2004).
[16] I. Gabitov, R. Indik, L. Mollenauer, M. Shkarayev, M. Stepanov, and P. M. Lushnikov, Opt. Lett. **32**, 605 (2007).
[17] J. P. Gordon and L. F. Mollenauer (private communication).
[18] A. Hause, H. Hartwig, B. Seifert, H. Stolz, M. Böhm, and F. Mitschke, Phys. Rev. A **75**, 063836 (2007).
[19] N. J. Smith, F. M. Knox, N. J. Doran, K. J. Blow, and I. Bennion, Electron. Lett. **32**, 54 (1996).
[20] S. Turitsyn, E. Shapiro, S. Medvedev, M. P. Fedoruk, and V. Mezentsev, C. R. Phys. **4**, 145 (2003).
[21] L. F. Mollenauer and J. P. Gordon, *Solitons in Optical Fibers: Fundamentals and Applications* (Academic Press, San Diego, 2006).
[22] L. F. Mollenauer, J. P. Gordon, and S. G. Evangelides, Opt. Lett. **17**, 1575 (1992).
[23] G. P. Agrawal, *Nonlinear Fiber Optics*, 4th ed. (Academic Press, San Diego, 2007).
[24] J. H. B. Nijhof, W. Forysiak, and N. J. Doran, IEEE J. Quantum Electron. **6**, 330 (2000).
[25] I. R. Gabitov and S. K. Turitsyn, Opt. Lett. **21**, 327 (1996).